

# Surfactant-induced conformational transition of amyloid $\beta$ -peptide

N. Sureshbabu · R. Kirubakaran · R. Jayakumar

Received: 1 August 2008 / Revised: 5 October 2008 / Accepted: 12 October 2008 / Published online: 13 November 2008  
© European Biophysical Societies' Association 2008

**Abstract** Accumulating evidence suggests that  $A\beta_{1-42}$ –membrane interactions may play an important role in the pathogenesis of Alzheimer's disease. However, the mechanism of this structural transition remains unknown. In this work, we have shown that submicellar concentrations of sodium dodecyl sulfate (SDS) can provide a minimal platform for  $A\beta_{1-42}$  self-assembly. To further investigate the relation between  $A\beta_{1-42}$  structure and function, we analyzed peptide conformation and aggregation at various SDS concentrations using circular dichroism (CD), Fourier transform infrared spectroscopy, and gel electrophoresis. These aggregates, as observed via atomic force microscopy, appeared as globular particles in submicellar SDS with diameters of 35–60 nm. Upon sonication, these particles increased in disc diameter to 100 nm. Pyrene  $I_3/I_1$  ratios and 1-anilinonaphthalene-8-sulfonic acid binding studies indicated that the peptide interior is more hydrophobic than the SDS micelle interior. We have also used Forster resonance energy transfer between N-terminal labeled pyrene and tyrosine (10) of  $A\beta_{1-42}$  in various SDS

concentrations for conformational analysis. The results demonstrate that SDS at submicellar concentrations accelerates the formation of spherical aggregates, which act as niduses to form large spherical aggregates upon sonication.

**Keywords** Alzheimer's disease ·  $A\beta_{1-42}$  peptide · Submicellar SDS concentration · Partially folded structures · FRET

## Abbreviations

$A\beta_{1-42}$	Amyloid $\beta$ peptide, a 42 residue peptide
AFM	Atomic force microscopy
ANS	1-Anilinonaphthalene-8-sulfonic acid ammonium salt
CD	Circular dichroism
FRET	Forster resonance energy transfer
FTIR	Fourier transformed infrared spectroscopy
SDS	Sodium dodecyl sulfate
TFA	Trifluoro acetic acid
TFE	2,2,2 Trifluoroethanol

**Electronic supplementary material** The online version of this article (doi:10.1007/s00249-008-0379-8) contains supplementary material, which is available to authorized users.

N. Sureshbabu · R. Jayakumar (✉)  
Bio-Organic and Neurochemistry Laboratory,  
Central Leather Research Institute,  
Adyar, Chennai 600 020, India  
e-mail: karkuvi77@yahoo.co.uk

N. Sureshbabu  
e-mail: nsureshh@gmail.com

R. Kirubakaran  
National Institute of Ocean Technology,  
Velacherry-Tambaram Main Road,  
Pallikaranai, Chennai 601302, India

## Introduction

The conformational transition of non-toxic amyloid  $\beta$ -peptide ( $A\beta$ ) into a protease-resistant toxic assembly in the brain is a significant step in the pathogenesis of Alzheimer's diseases (Selkoe 1996; Finelli et al. 2004). A thorough understanding of this transformation is essential to learn more about the onset of the disease and, at the same time, challenges our chemical intuition. It was shown that soluble  $A\beta_{1-42}$  oligomers are more toxic than monomeric and fibrillar  $A\beta_{1-42}$  (Rochet and Lansbury 2000). Spectroscopic studies indicated that these oligomers

consist of molten globule-like portions with equilibrating secondary structures (Uversky and Fink 2004). The molten globules with less ordered, metastable intermediates exhibited protease K resistance, preferential membrane internalization, and accumulation in human glial cells (Matsunaga et al. 2002). The metastable intermediate appears to share most of the characteristics featured by other amyloidogenic sequences. The latter are comprised in proteins such as phosphoglycerate kinase (Guijarro et al. 1998), cystatin C (Ekiel and Abrahamson 1996), acylphosphatase (Chiti et al. 1999), transthyretin (Lai et al. 1996),  $\alpha$ -synuclein (Uversky et al. 2001) and prion (Booth et al. 1997; Prusiner 1997; Fezoui and Teplow 2002) that have been shown to collapse into a “molten globule” form in which the hydrophobic residues are shielded from the aqueous environment. Subsequent changes in secondary and tertiary structures result in the formation of soluble oligomers.

The influence of the microenvironment on the assembly of soluble oligomers from misfolded monomeric proteins is not well understood. Several metabolites have been invoked to explain this process. Interestingly, diffusible, nonfibrillar  $A\beta_{1-42}$  in association with membrane components has been shown to have neurotoxic properties (Kirkitadze et al. 2002; Klein 2002; Walsh et al. 2002; Lambert et al. 1994). Furthermore, Selkoe et al. observed that freshly exocytosed  $A\beta_{1-42}$  can instantaneously develop into characteristically toxic structures (Selkoe 1996). It is possible that the spatially constrained lipid environment of  $A\beta_{1-42}$  during exocytosis could be the reason for the instantaneous structure development in this peptide. Yamamoto et al. found that concentrations of SDS near the critical micelle concentration (cmc 0.7 mM) stabilize soluble beta2-microglobulin oligomers and induce enhanced fibril growth at neutral pH (Yamamoto et al. 2004). Recently, Rangachari et al. observed  $A\beta_{1-40}$  aggregation in the presence of 2 mM SDS after 12 days of incubation (Rangachari et al. 2006, 2007). Tew et al. have shown that submicellar concentrations of SDS induce conformational changes from random coil through a  $\beta$ -sheet-rich intermediate to an  $\alpha$ -helix end point (Tew et al. 2008). At submicellar concentrations, SDS is known to enhance the enzymatic activity of many systems. At these levels, SDS mimics the function of phospholipid flat domains by inducing conformational changes in enzymes (Decker et al. 2001; Muga et al. 1993; Jao et al. 2004). For example, two ancient species of chelicerate, *Limulus polyphemus* and *Eurypelma californicum*, develop odiphenoloxidase activity in response to submicellar concentrations of SDS, a reagent commonly used to identify phenoloxidase activity (Decker et al. 2001). Surfactant micelles can effectively be applied to simulate the catalytic role of the membrane and investigate the conformational properties of hormones,

particularly for proteins such as calcitonin at the interface (Schwyzer 1986; Motta et al. 1998).

We have chosen this study to investigate the effect of submicellar SDS concentrations on the conformational and amyloidogenic behavior of  $A\beta_{1-42}$  peptide. High levels of turbidity and light scattering are normally encountered in lipid–peptide interaction studies, making spectroscopic measurement more difficult. A submicellar concentration of SDS solution greatly reduces turbidity and light scattering for better spectroscopic measurement (Garavito and Ferguson-Miller 2001). Although recent studies of amyloid peptide at low SDS concentration have reported on the conformational transition and morphology of the large aggregates formed, the detailed conformational properties of the intermediate state (partially folded intermediate) will be more important to understand the mechanism of aggregation (Yamamoto et al. 2004; Rangachari et al. 2006, 2007). Here, we focus on elucidating the details on the structure of the partially folded intermediates formed at submicellar SDS concentrations and its relationship to amyloid abeta oligomers present in the AD brain.

Sonication is yet another method frequently used to induce amyloid aggregates in  $A\beta$  amyloids (O’Nuallain et al. 2004), polyglutamines (Chen et al. 2001), prions (Soto 2001), and  $\alpha$ 1-antichymotrypsin (Crowther et al. 2003), as well as proteins not associated with disease (Ramirez-Alvarado et al. 2000). Although the effects of sonication and detergents on the development of aggregates have been studied (De planque et al. 2007), their role in the formation of oligomers and protofibrils still awaits closer inspection. Here, we examine the combined effects of SDS and ultrasonication on the monomeric  $A\beta_{1-42}$  peptide, and our results show that SDS at submicellar concentrations accelerates the formation of flat domains in  $A\beta_{1-42}$  aggregates.

## Materials and methods

### Peptide synthesis and characterization

The peptide  $A\beta_{1-42}$  (DAEFRHDSGYEVHHQKLVFF AEDVGSNKGAIIGLMVGGVVIA) was synthesized with solid phase chemistry using 4-hydroxymethylphenoxy acetyl (Wang) resin and Fmoc protected amino acids together with either 1-hydroxy benzotriazole (HOBt) or *N,N*-dicyclohexyl carbodiimide (DCC) as a coupling agent. The pyrene-labeled peptide was synthesized by adding the pentafluorophenol ester of 1-pyrenebutyric acid to the deprotected N-terminus of resin-bound  $A\beta_{1-42}$ . Peptides were cleaved off the resin with trifluoromethane sulfonic acid/thioanisole/ethanedithiol/TFA (1:1:1:7) and precipitated with cold ether. The peptide composition was

determined using the phenyl isothiocyanate (PITC) method and its mass confirmed by matrix-assisted laser desorption ionization (MALDI) mass spectrometry. The peptide was >90% pure as judged by HPLC and the molecular weight was 4514.14 (M+H)<sup>+</sup>. All reagents used in peptide synthesis were of the purest analytical grade. Pentafluorophenol was from Spectrochem Pty. Ltd, Mumbai, *N,N*-dicyclohexyl carbodiimide, SDS, TFA and HOBt were from Sigma Aldrich, and Fmoc amino acids were from Novabiochem.

#### Peptide solutions

The newly synthesized peptide was processed as previously described (Ma et al. 1997). Briefly, A $\beta$ <sub>1–42</sub> was incubated with TFA–TFE (1:5) for 2 h. The solvent was then removed completely under a stream of nitrogen, dissolved in PBS and centrifuged at 10,000 rpm. The supernatant was frozen in liquid nitrogen and lyophilized. The white solid was stored at –70°C until needed. Before any series of experiments, a stock solution was freshly prepared by dissolving the lyophilized peptide in phosphate buffered saline (PBS 10 mM phosphate buffer, 150 mM sodium chloride, pH 7.4) to a final concentration of 1 mg/ml (220  $\mu$ M). When required, aliquots of this stock solution were diluted with different amounts of 50 mM SDS and the volume adjusted with PBS to reach the desired concentrations.

#### Determination of the cmc

Conductivity measurements were made using an Elico conductivity meter, Hyderabad, India. The temperature of the cell compartment was regulated using a thermostat. For the determination of the cmc, different concentrations of SDS in the absence and presence of A $\beta$ <sub>1–42</sub> peptide were prepared in PBS. The specific conductance of the solution was recorded. The abrupt change in the initial slope value at a particular concentration (2 mM SDS) was considered to be the cmc.

#### Circular dichroism (CD)

Spectra were acquired with a JASCO J-715 spectropolarimeter (UK) equipped with a thermostated cell holder, using a quartz cell of 1-mm path length at 25°C. This instrument was calibrated using ammonium-d<sub>10</sub>-camphor sulfonic acid as recommended by the instrument manufacturer. Spectra were collected over the wavelength range 198–250 nm with a 1 nm bandwidth. For each spectrum, five scans were collected and averaged. The averaged data were then corrected for background and smoothed using Jasco J-715 software supplied by the manufacturer. The CD values were expressed using molar ellipticity. Quantitative estimation of

secondary structure was obtained using the computer program CONTINLL, included in the CDpro package.

#### Fourier transformed infrared spectroscopy (FT-IR)

FTIR spectra were recorded using a Nicolet 320 Avatar spectrometer (New York, USA) at 25°C. Measurements were performed using the same solutions employed in the CD studies. In the event, a drop of A $\beta$ <sub>1–42</sub>–SDS solution was applied on a ZnSe plate which was then placed in a flask, frozen in liquid nitrogen, and evacuated. After lyophilization, FTIR spectra were recorded between 400 and 4,000 cm<sup>–1</sup>; the air background was subtracted; and the resulting baseline smoothed. Spectra analysis was performed with GRAMS/LT (Galactic Industries) and limited to the 1,600–1,700 cm<sup>–1</sup> range since the latter comprises the very characteristic amide I absorption band. The secondary structure content was determined after deconvolution of this spectral region.

#### Gel electrophoresis

A $\beta$ <sub>1–42</sub> samples prepared as described above were used immediately for gel electrophoresis. A $\beta$ <sub>1–42</sub> samples were diluted in NuPage sample buffer and separated by SDS-PAGE on a 12% NuPage Bis–Tris gel (Invitrogen, Eugene, USA) for a period of 3 h with a uniform current of 40 mA. The resolved A $\beta$ <sub>1–42</sub> aggregates were then transferred to a polyvinylidene difluoride membrane (Invitrogen) and this blocked with 5% (w/v) nonfat dry milk in TBS/0.05% Tween 20 for 1 h. The membrane was then incubated with 6E10 (1:3,000), a mouse monoclonal A $\beta$  antibody for residues 1–17 (Signet, Dedham, MA). After labeling with horseradish peroxidase-conjugated goat Ig anti-mouse antibody (1:5,000, Pierce), signals were developed using enhanced chemiluminescence (ECL, Amersham Biosciences, USA), and visualized with an Eastman Kodak Co. 440 CF Image Station (Perkin-Elmer Life Sciences). Molecular mass was estimated by referencing to Rainbow molecular weight markers (Amersham Biosciences) as described in Fig. 2.

#### Atomic force microscopy

Samples were imaged with a Shimadzu-5500 atomic force microscope (AFM; Shimadzu, Kyoto, Japan), using a Si<sub>3</sub>N<sub>4</sub> tip and the tapping-scanning mode. The tube scanner was a 30- $\mu$ m scan master. Samples were prepared for AFM imaging by depositing a 10- $\mu$ l aliquot of peptide–SDS mixture on freshly cleaved mica. After drying with a stream of nitrogen, the surface was washed once with double-distilled water to remove buffer salts and detergent, and dried again.

## Fluorescence measurements

All fluorescence measurements were performed on a Perkin Elmer LS 45 Luminescence spectrometer (USA) with an excitation and emission band pass of 5 nm using a semi-micro quartz cuvette with a 1-cm path length. The light source was a Xenon lamp.

### Intrinsic fluorescence

The single tyrosine residue, at position 10 of A $\beta$ <sub>1–42</sub> was excited at 275 nm and its fluorescence was monitored in the range from 290 to 350 nm. Peptide concentrations for intrinsic fluorescence measurements were kept at 25  $\mu$ M.

### Acrylamide quenching

The intrinsic tyrosine fluorescence was quenched by adding aliquots of the quencher from a stock solution into a quartz cuvette containing 25  $\mu$ M A $\beta$  peptide. Fluorescence intensities were corrected for dilution effects. Data were analyzed using the general form of the Stern–Volmer equation (Eq. 1),

$$I_0/I = 1 + K_{SV}[Q] \quad (1)$$

$I_0$  and  $I$  are the fluorescence intensities in the absence and presence of quencher, respectively;  $K_{SV}$  is the quenching constant and  $Q$  the quencher concentration.

### Pyrene $I_3/I_1$ ratio

Fluorescence spectra were recorded for fixed concentrations of peptide and pyrene with different concentrations of SDS. Pyrene was solubilized with SDS. Specifically, the desired amount of pyrene ( $5 \times 10^{-7}$  M in MeOH) was placed in an Eppendorf tube and dried under a stream of nitrogen. The solid was then re-dissolved in PBS containing 0–5 mM SDS and the mixture vortexed until a clear solution was obtained. The sample was finally supplemented with A $\beta$ <sub>1–42</sub> so that the final concentrations were 25  $\mu$ M peptide and 0.5  $\mu$ M pyrene. To ensure thorough mixing, the solution was vigorously vortexed. The emission spectrum from 350 to 600 nm was collected with excitation at 335 nm. For micropolarity measurements, fluorescence intensities at  $I_1$  (373 nm) and  $I_3$  (383 nm) were recorded using a sample cell of 10 mm path length.

Calculation of distance between the fluorophores in Py-A $\beta$ <sub>1–42</sub>

To study the folding behavior of A $\beta$ <sub>1–42</sub>, intramolecular FRET was investigated for its pyrene-conjugate. We

choose the ratio of 1:10 between the labeled and unlabeled peptide in order to avoid the possible contributions from intermolecular FRET (Kim and Lee 2004). Tyrosine at position 10 was used as the energy donor and pyrene at the N-terminus as the acceptor.

We calculated efficiency of energy transfer ( $E$ ), forester radius ( $R_0$ ) and distance between the two probes ( $r$ ) from equations used by earlier workers in the field (Narayanan et al. 1993, 2001).

### ANS binding

A stock solution of 1 mM ANS was prepared in distilled, deionized water. ANS was added to samples such that its final concentration was 100-fold lower than that of A $\beta$ <sub>1–42</sub>. Control solutions with ANS and SDS but no peptide were prepared and their spectra subtracted from those acquired with solutions containing ANS and either peptide–SDS or peptide alone. Only in the latter case, the emission value was proportional to the concentration of ANS. The maximum change in emission upon aggregation was observed at 460 nm. The emission spectra were collected from 390 to 600 nm upon excitation at 375 nm.

## Results

According to previous studies, freshly prepared soluble A $\beta$ <sub>1–42</sub> peptide is reported to be flexible and primarily unstructured in aqueous solutions (Fezoui and Teplow 2002). At submicellar concentrations (around the cmc) SDS favors partially folded conformers, which represent key intermediates in the amyloid aggregation process (Yamamoto et al. 2004). Since there are numerous studies on the structure of amyloid  $\beta$  peptide in SDS micelles (Shoa et al. 1999; Coles et al. 1998), we focused our attention on aggregates formed at submicellar SDS concentrations and examined whether A $\beta$ <sub>1–42</sub> adopts a non-helical amyloid-like structure at these concentrations.

Studies on the conformational transition of A $\beta$ <sub>1–42</sub> peptide at different SDS concentration

CD and IR measurements were performed to investigate folding and conformational changes of A $\beta$ <sub>1–42</sub> at premicellar and postmicellar concentrations of SDS. Figure 1a shows the CD spectra of A $\beta$ <sub>1–42</sub> peptide in an SDS-free environment (curve a), with 0.5 mM SDS (curve b), 1.5 mM SDS (curve c) and 1.5 mM SDS followed by sonication (curve d). The contribution of each secondary structure was calculated using the CONTINLL program (Sreerama and Woody 2000) and the values obtained from this analysis are listed in Table 1.

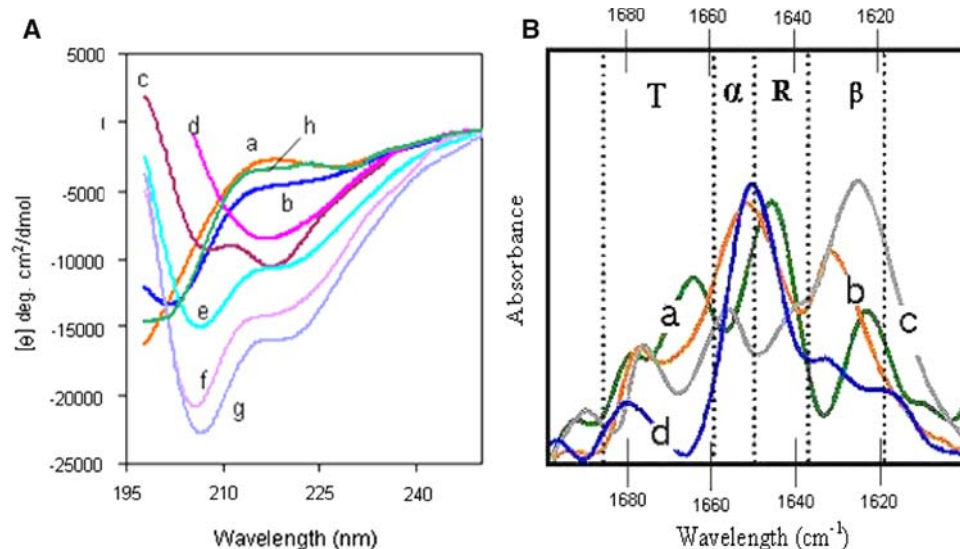


**Fig. 1** **a** CD analysis of  $A\beta_{1-42}$  secondary structure as a function of SDS concentration. Spectra of 25  $\mu\text{M}$   $A\beta_{1-42}$  in PBS were recorded at 298 K in the absence (**a**) and presence of 0.5, 1.5, 2.0, 4.0 and 5.0 mM SDS (**b, c, e, f, g**, respectively). Spectra of  $A\beta_{1-42}$  alone (**h**) and  $A\beta_{1-42}$  in the presence of 1.5 mM SDS (**d**) were also obtained after the respective samples had been sonicated for 15 s. The fractional secondary structure corresponding to each peptide sample was obtained from deconvolution of the CD spectrum using the

CDpro program CONTINLL. The results of this analysis are presented in Table 1. **b** FTIR analysis of  $A\beta_{1-42}$  secondary structure as a function of SDS concentration; 50  $\mu\text{l}$  aliquots of the samples designated *a, c, d* and *g* for the CD experiments in **a** was each applied to a ZnSe plate, frozen and lyophilized. FTIR spectra were recorded at 298 K. Spectra were deconvoluted using GRAMS/LT Thermo galactic software and the resulting secondary structure data presented in Table 1

**Table 1** Estimation of  $A\beta_{1-42}$  secondary structure as a function of SDS concentration

Peptide/surfactant	$\alpha$ -Helix %	$\beta$ -Sheet %	$\beta$ -Turn %	Unordered %
Estimation of secondary structure from CD measurements (Fig. 1a) by CONTINLL software				
$A\beta_{1-42}$ alone	$10.7 \pm 0.3$	$17.2 \pm 0.5$	$19.1 \pm 0.5$	$53.0 \pm 2$
$A\beta_{1-42}$ + 0.5 mM SDS	$13.2 \pm 0.25$	$27.2 \pm 0.7$	$15.6 \pm 0.55$	$44.0 \pm 1.7$
$A\beta_{1-42}$ + 1.5 mM SDS	$33.1 \pm 1.0$	$25.8 \pm 0.8$	$14.3 \pm 0.3$	$26.8 \pm 0.7$
$A\beta_{1-42}$ + 1.5 mM-SDS sonication	$11.8 \pm 0.2$	$48.0 \pm 1.8$	$16.0 \pm 0.4$	$24.2 \pm 0.1$
$A\beta_{1-42}$ + 2.0 mM SDS	$41.8 \pm 0.5$	$18.2 \pm 0.25$	$14.8 \pm 0.3$	$25.2 \pm 0.8$
$A\beta_{1-42}$ + 4.0 mM SDS	$50.9 \pm 1.5$	$14.8 \pm 0.33$	$12.3 \pm 0.25$	$22.0 \pm 0.3$
$A\beta_{1-42}$ + 5.0 mM SDS	$55.2 \pm 2.0$	$18.3 \pm 0.45$	$10.5 \pm 0.2$	$16.0 \pm 0.55$
Estimation of secondary structure from FT-IR measurement (Fig. 1b) by GRAMS/LT software				
$A\beta_{1-42}$ alone	$9.3 \pm 0.2$	$19.8 \pm 0.55$	$30.9 \pm 1.0$	$40 \pm 1.5$
$A\beta_{1-42}$ + 1.5 mM SDS	$29.8 \pm 0.8$	$31.7 \pm 0.6$	$15.7 \pm 0.25$	$22.8 \pm 0.9$
$A\beta_{1-42}$ + 1.5 mM-sonicated	$18.9 \pm 0.4$	$48.7 \pm 1.0$	$22.4 \pm 0.4$	$10.0 \pm 0.2$
$A\beta_{1-42}$ + 5 mM SDS	$46.5 \pm 1.0$	$15.7 \pm 0.25$	$20.3 \pm 0.4$	$17.5 \pm 0.3$

Data were obtained by deconvoluting the CD spectra in Fig. 1a and FTIR spectra in Fig. 1b using the CDpro program CONTINLL and GRAMS/LT software program, respectively

The CD spectrum of SDS-free  $A\beta_{1-42}$  is typical of a peptide containing significant portions of random-coil structure as evidenced by a curve with a characteristic minimum at 198 nm. Shoulder peaks that appear around 225 nm indicate a minor contribution from a  $\beta$ -sheet/turn structure, in agreement with an earlier observation (Terzi et al. 1995). The estimation of secondary structure shows that SDS-free  $A\beta$  consists of 53% random coil, 17%  $\beta$ -sheet, 19% turn, and 10%  $\alpha$ -helix. Addition of 0.5 mM

SDS decreased the contribution from unstructured peptide that rearranged to form  $\alpha$ -helix and  $\beta$ -sheet (curve *b*). Interestingly, Tew et al. also observed that  $A\beta_{1-40}$  and  $A\beta_{1-42}$  underwent conformational transition to more  $\beta$ -sheet structures at sub-micellar SDS concentrations (Tew et al. 2008). Specifically, the  $\beta$ -sheet contribution increased to 27% and the  $\alpha$ -helix to 13% (Table 1). At higher SDS concentrations, the CD spectrum indicates a major conformational transition from a largely disordered structure to



one highly enriched in  $\alpha$ -helices, the latter featuring 55% of the peptide at 5.0 mM SDS.

At 1.5 mM SDS, a notable change occurred in the CD spectrum (curve *c*), indicating a crossover at 200 nm and two minima located at 208 and 218 nm. This suggests a substantial degree of helical structures. However, the positions of the negative peaks are shifted from typical  $\alpha$ -helical conformations by  $\sim 3$  nm. At post-micellar SDS concentrations,  $A\beta_{1-42}$  clearly adopts a helical structure, with double minima at 206 and 222 nm (Fig. 1a curves *e*, *f*, *g*).

Our previous studies indicated that sonication of amyloid protein resulted in development of  $\beta$ -sheet structure (Satheeshkumar and Jayakumar 2002). Sonication is known to produce energy rich vapor–liquid interfaces in the liquid resulting in a shear force due to cavitation effects. Similarly, sonication or agitation has been reported to induce aggregation in blood and latex solutions (Loughheed et al. 1980; Jen and McIntire 1984). Shearing due to sonication can also align long chain molecules such as polymers, promoting their ability to interact with each other (Le Berre et al. 1998). Furthermore, upon sonication, a range of structurally diverse proteins resulted in aggregates that had tinctorial and structural properties similar to those of amyloid (Stathopoulos et al. 2004). Interestingly, we found that  $A\beta_{1-42}$  in 1.5 mM SDS instantaneously developed a substantial amount of  $\beta$ -sheet structure upon sonication. The two negative peaks at 208 and 218 nm (Fig. 1a, curve *c*) disappeared and were replaced by a single minimum at 217 nm (Fig. 1a, curve *d*). It should be noted that sonication alone in the absence of SDS did not induce any conformational change (curve *h*). Furthermore, sonication above the postmicellar concentration did not disturb the stable  $\alpha$ -helical secondary structure (data not shown). Similar structural changes from partially folded  $\alpha$ -helical structure to  $\beta$ -sheet structure at submicellar SDS concentration have been reported for SCR 3 peptide within 3 h of incubation (Pertinhez et al. 2002). In another study, it was observed that  $A\beta_{1-42}$  peptide undergoes a rapid conformational transition from  $\alpha$ -helix to  $\beta$ -sheet in 20% TFE (Fezoui and Teplow 2002). This result was interpreted as indicative of the formation of a partially folded helical intermediate in the transition from natively unfolded  $A\beta_{1-42}$  monomers to  $\beta$ -amyloid fibrils (Fezoui and Teplow 2002). Monomeric SDS surrounds proteins and lowers the dielectricity of their environment that persists in the protein interior (Waterhous and Johnson 1994).

More detailed information about SDS- and sonication-associated conformational changes in  $A\beta_{1-42}$  was obtained with FTIR. Infrared spectroscopy has been long used to study alterations in protein conformation and to quantify protein secondary structures (Dong et al. 1995). The FTIR spectra of  $A\beta_{1-42}$  at different SDS concentrations are

shown in Fig. 1b. Each type of secondary structure was estimated by a deconvolution method and is listed in Table 1. The IR spectrum of the amyloid  $\beta$  peptide in the absence of SDS shows a predominant band at  $1,645\text{ cm}^{-1}$  due to C=O stretching (amide I) and is typical of a random coil conformation (Fig. 1b, curve *a*). The weak band at  $1,622\text{ cm}^{-1}$  and bands at  $1,665$ – $1,695\text{ cm}^{-1}$  have been generally assigned to the  $\beta$ -sheet and  $\beta$ -turn conformations. However, in the presence of 1.5 mM SDS, a new intense peak appeared at  $1,653\text{ cm}^{-1}$ , typical of  $\alpha$ -helical structure (Fig. 1b, curve *b*). Bands at  $1,631$  and  $1,678\text{ cm}^{-1}$  are indicative of intermolecular  $\beta$ -sheet and  $\beta$ -turn structures (Halverson et al. 1990; Surewicz et al. 1993). This result is in good agreement with the CD data. Sonication in the presence of 1.5 mM SDS led to a loss of  $\alpha$ -helicity as indicated by the decreased absorbance at  $1,653\text{ cm}^{-1}$  and concomitant enrichment in  $\beta$ -sheet structure as shown by a more intense band at  $1,625\text{ cm}^{-1}$  (Fig. 1b, curve *c*). These changes are attributed to peptide aggregation and strong intermolecular  $\beta$ -sheet formation. The IR spectrum of peptide in the presence of 5 mM SDS reveals a very intense peak at  $1,652\text{ cm}^{-1}$ , suggesting that the peptide exists as a stable  $\alpha$ -helical structure (Fig. 1b, curve *d*). Overall, the IR results are in agreement with and support those obtained by CD analysis (Fig. 1a).

#### Gel electrophoresis

We next sought to identify the nature of the aggregates obtained by treatment of the amyloid peptide with SDS. Western blot analysis of freshly prepared  $A\beta_{1-42}$  solutions in the absence of SDS revealed the presence of monomers, trimers and tetramers (Fig. 2, lane 1). With 1.5 mM SDS, two additional bands were resolved by PAGE: a large aggregate of molecular weight  $\sim 50$  kDa attributed to a 12-mer (lane 2); and a lighter entity around molecular weight 20 kDa. Analysis of the peak intensities, quantified with Image software, indicated that abundance of oligomers was relatively higher in the presence of SDS than in its absence (Fig. 2b). Sonication had no effect on the band pattern; instead, it increased further the intensity of the tetramer peak (Fig. 2a, lane 3). These findings are in agreement with a recent observation. In that instance, it was shown that extracts from AD brains contained a major oligomer at  $\sim 56$  kDa as well as lower molecular weight oligomeric species assigned to 4-mers (Gong et al. 2003).

#### Atomic force microscopy

In order to define further the nature of the aggregated species, an analysis of their morphologies was carried out using AFM. AFM analysis on the assemblies produced at submicellar SDS concentrations (1.5 and 1.5 mM SDS

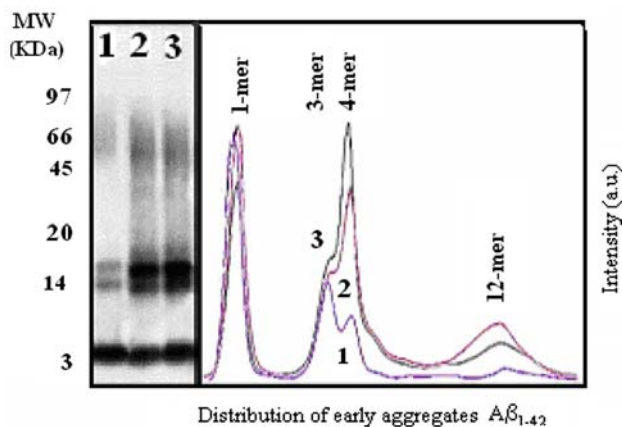


**Fig. 2** Western analysis of  $A\beta_{1-42}$ . **a** Western blot images of  $A\beta_{1-42}$ . The material originally loaded into the gel lanes corresponds to 25  $\mu$ M  $A\beta_{1-42}$  alone (lane 1), in the presence of 1.5 mM SDS (lane 2) and in the presence of 1.5 mM SDS following 15 s sonication of the sample (lane 3). **b** Densitometric traces of lanes 1, 2 and 3 from **a**. The data are plotted as intensity versus distance

followed by sonication) reveals globular aggregates ranging in size from 35 to 60 nm and from 100 to 200 nm, respectively (Fig. 3a, b, respectively).

#### Forster resonance energy transfer (FRET)

FRET has long been used as a spectroscopic ruler to give accurate measures of distances within proteins and other macromolecules (Stryer 1978). The intrinsic fluorophores of proteins and peptides provide conformational probes to monitor structural transitions and unfolding (Wu et al. 1994). For these reasons, more information on the conformation of the  $A\beta_{1-42}$  peptide at submicellar SDS levels was obtained by monitoring FRET between tyrosine at position 10 and a pyrene acceptor covalently linked at the N-terminus of the  $A\beta_{1-42}$  peptide. In fact, the N-terminal region is known for its crucial participation in the folding of  $A\beta$  as shown by studies using specific monoclonal antibodies (Solomon 2002).

To better understand the roles played by SDS and sonication in the folding of the  $A\beta_{1-42}$  peptide, fluorescence emission spectra were recorded under different conditions: no SDS, 1.5 mM SDS, and 1.5 mM SDS with sonication (Fig. 4, curves labeled with *d*, *e*, and *f*). The distances between the two fluorophores were calculated from the spectra as described under “Materials and methods” and are reported in Table 2. In the absence of SDS, the calculated distance was  $\sim 22$  Å and decreased to 17–18 Å at submicellar SDS. Sonication had little effect on the distance between the donor and the acceptor. This comes to odds with our CD and IR results that show the peptide adopts a  $\beta$ -sheet conformation when subjected to SDS and sonication. Generally, formation of  $\beta$ -sheet is accompanied by an increase in

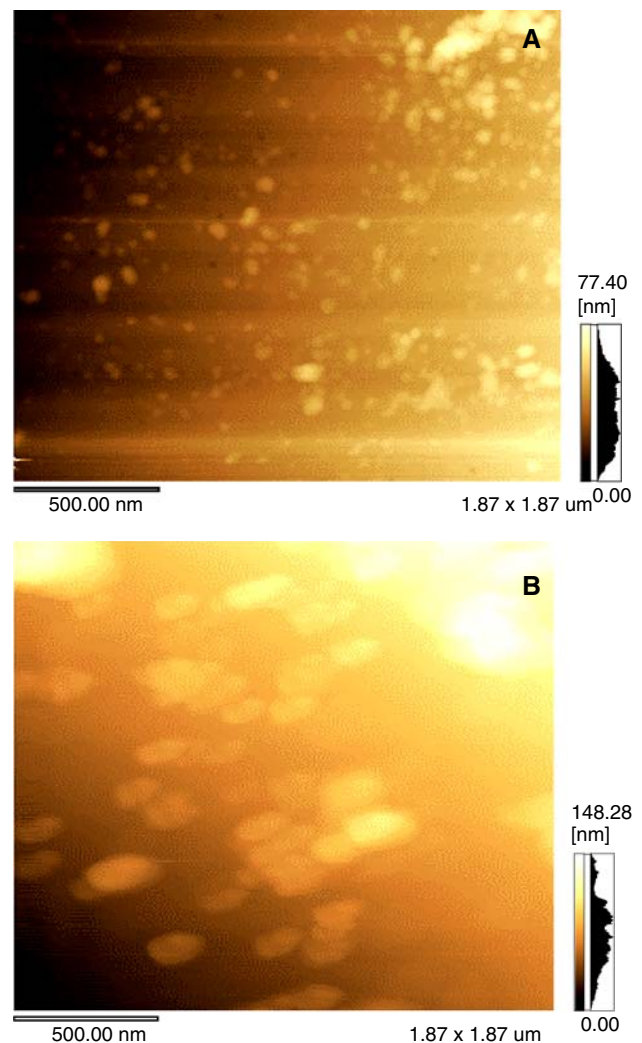


**Fig. 3** AFM analysis of  $A\beta_{1-42}$ . Samples of 25  $\mu$ M  $A\beta_{1-42}$  in the presence of 1.5 mM SDS were either untreated (**a**), or subjected to 15 s sonication (**b**) before being deposited onto a mica surface and desiccated under a stream of nitrogen gas. AFM data were collected in tapping mode. The images represent an area of  $\sim 3.5$   $\mu$ m<sup>2</sup>. The length of the scale bar represents 500 nm. The particle size was estimated from its cross sectional height

intramolecular fluorophore distances (Narayanaswami et al. 1993). Recently, Gehman et al. from solid state NMR studies investigated that  $A\beta_{1-42}$  peptide in the presence of phospholipids showed an increase in  $\beta$ -sheet at the C-terminus, which would be consistent with the CD and FRET data, i.e. the increase in  $\beta$ -sheet is not necessarily at the N-terminus (Gehman et al. 2008). Using ArgusLab-software, a molecular model was generated for an extended  $\beta$ -sheet and an estimated donor–acceptor distance of 32 Å was obtained (Table 3, entry 1). Models with partially folded conformations such as  $\alpha$ -helix or  $\beta$ -hairpin furnished values closer to though different from the observed *r* value (Table 3, entries 2 and 4, respectively). When a  $\beta$ -helix was considered, the estimated pyrene-tyrosine distance approached 17 Å

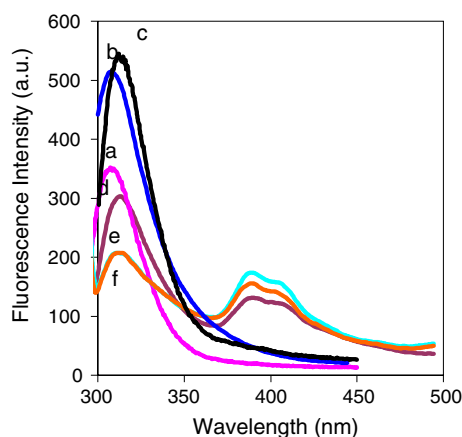


**Fig. 4** Fluorescence emission spectra of  $A\beta_{1-42}$  (donor alone), Py- $A\beta_{1-42}$  (donor-acceptor) in PBS. Data were collected at 298 K using 275 and 335 nm excitation and represent 25  $\mu$ M Py- $A\beta_{1-42}$ . The labels in spectra (a) donor alone in SDS-free (b) donor alone in the presence of 1.5 mM SDS (c) in the presence of 1.5 mM SDS following 15 s sonication of the sample (d) donor-acceptor in SDS-free (e) donor-acceptor in the presence of 1.5 mM SDS and (f) in the presence of 1.5 mM SDS following 15 s sonication of the sample

(Table 3, entry 3). Among all the possible conformers, monomer is likely to adopt the most “extended” peptide stretch.

#### Acrylamide quenching studies

Information on the aggregation state of the  $A\beta_{1-42}$  peptide was obtained by examining the accessibility of neutral and cationic quenching agents to the tyrosine donor at position 10. Acrylamide was tested at submicellar SDS concentrations before and after sonication. The Stern–Volmer constants ( $K_{SV}$ ) were calculated using the data from Fig. 5a as described under “Material and methods” and are listed in Table 4.

Acrylamide is a polar, uncharged quencher that, in the aqueous phase, interacts with all surfaces independently of their charge. When acrylamide was used, the  $K_{SV}$  value decreased from 5.77 to 5.11  $M^{-1}$  upon addition of SDS (Fig. 5a; Table 4). A lower  $K_{SV}$  value was interpreted as a reorganization of the peptide, at least at the N-terminus, to form a more compact structure in which tyrosine is less exposed to the surrounding medium. That the N-terminus

of soluble monomeric  $A\beta_{1-42}$  is more exposed to the aqueous environment was shown by Chaney et al. (1998). When the same experiment was repeated for sonicated SDS–peptide mixtures, the calculated constant was 4.8  $M^{-1}$ . Upon sonication, the size of the aggregates increases as shown by AFM, implying that less protein surface and hence tyrosine residues become available to acrylamide quenching.

#### Determination of the nature of the complex formed by SDS and $A\beta_{1-42}$

We employed pyrene as an external fluorescence probe to investigate firstly the nature of complex formed between SDS–amyloid  $\beta$ -peptide and secondly on the polarity of the interior of the aggregate. The vibrational fine structure of the fluorescence emission of pyrene was therefore assessed at different SDS concentrations. Pyrene emission intensity is known to be an indicator of the solvent polarity around a fluorophore. Increase in the  $I_3/I_1$  ratio is diagnostic of a decrease in the polarity of the microenvironment surrounding the probe.

Figure 5b shows the vibrational fine structure ( $I_3/I_1$ ) of pyrene fluorescence as a function of the SDS concentration in the absence and presence of amyloid  $A\beta_{1-42}$  peptide. With no peptide and SDS below its cmc, the  $I_3/I_1$  ratio equals 0.52, suggesting that the pyrene molecules are exposed to the aqueous phase. A sharp increase of  $I_3/I_1$  from 0.52 to 0.83 was observed at the cmc of SDS. No further increase was observed above the cmc due to micelle formation. For the  $A\beta_{1-42}$  peptide alone, the  $I_3/I_1$  polarity ratio is around 0.70. This indicates that the pyrene probe associates with hydrophobic residues of the peptide, albeit to a lesser extent than with the SDS micelles. As expected, the simultaneous presence of SDS and peptide led to a further increase in the  $I_3/I_1$  polarity ratio: 0.96 with sonication and 0.93 without. On the other hand, below the cmc, pyrene favors the peptide over SDS ( $0.70 > 0.52$ ), presumably due to stabilizing effects such as  $\pi$ -stacking with the aromatic moieties present in the peptidic chain. Thus, SDS micelles and peptide together, synergistically improve the creation of a hydrophobic core ( $0.93 > 0.83$  and  $0.93 > 0.70$ ).

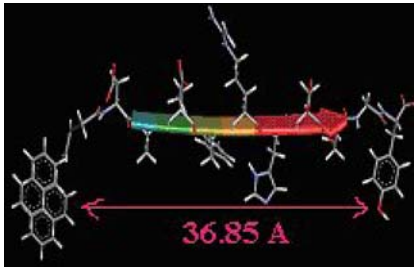
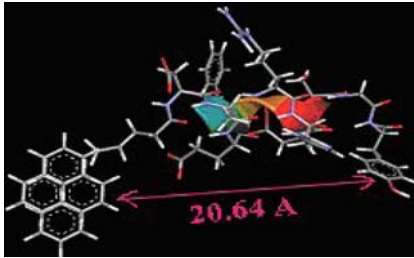
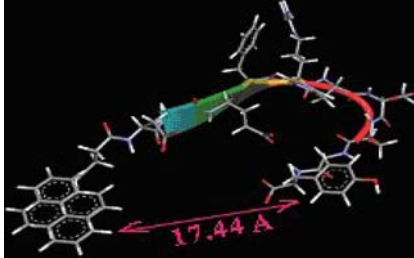
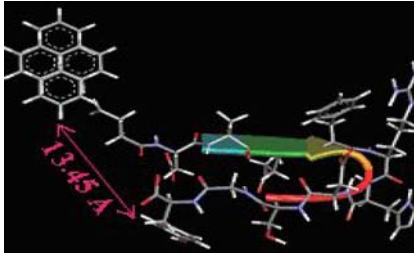
**Table 2** FRET analysis of Py- $A\beta_{1-42}$

Parameters	SDS-free $A\beta_{1-42}$	1.5 mM SDS $A\beta_{1-42}$	1.5 mM SDS-sonication $A\beta_{1-42}$
$J$ ( $cm^3 M^{-1}$ )	$7.02 \times 10^{-15}$	$8.98 \times 10^{-15}$	$9.05 \times 10^{-15}$
$E$	$0.15 \pm 0.04$	$0.58 \pm 0.07$	$0.60 \pm 0.08$
$Q$	$0.031 \pm 0.01$	$0.038 \pm 0.01$	$0.037 \pm 0.01$
$R_0$ (Å)	$16.49 \pm 0.07$	$17.78 \pm 0.09$	$17.73 \pm 1.2$
$r$ (Å)	$22.03 \pm 1.1$	$16.84 \pm 0.8$	$16.54 \pm 0.07$

$R$  values correspond to distances between the tyrosine 10 donor and N-terminal pyrene acceptor



**Table 3** FRET values based on various models generated using ArgusLab

Entry	Model	Calculated distance using model (Å)	Molecular models
1	$\beta$ -Sheet for A $\beta_{1-10}$ residues + pyrene 1-butyric acid	$32.06 \pm 5$	
2	$\alpha$ -Helix for A $\beta_{1-10}$ residues + pyrene 1-butyric acid	$16.13 \pm 5$	
3	$\beta$ -Helix for A $\beta_{1-10}$ residue 16 residue rung + pyrene 1-butyric acid	$14.32 \pm 5$	
4	$\beta$ -Hairpin for A $\beta_{1-10}$ residues + pyrene 1-butyric acid	$9.13 \pm 5$	

We built up the polypeptide chain gradually by incrementing the aminoacid residues with suitable phi and psi torsional angles (Mark)

### ANS fluorescence

ANS is frequently used as a probe to demonstrate the presence of partially folded conformations in proteins and peptides, since it binds to portions of the macromolecule that are shielded from the solvent (Kayed et al. 1999). Figure 6 (curve *a*) indicates that in an aqueous system, the emission maximum of ANS occurs at 520 nm. With freshly prepared solutions of monomeric peptide in the absence of SDS, we see minimal changes in ANS spectra indicating the least binding with the unordered conformation (curve *b*). The same was true even upon sonication of the freshly soluble peptide in the absence of SDS (curve *c*). However, in the presence of 1.5 mM SDS, fluorescence emission increased with a blue shift of 30 nm relative to dye alone

(Fig. 6, curve *d*). Even more pronounced changes were observed upon sonication (higher fluorescence emission as well as 42 nm blue shift), indicating further solvent protection of the dye-binding site in the peptide aggregate (Fig. 6, curve *e*) (Kelly 1998).

### Discussion

The  $\beta$ -amyloid peptides are known to strongly interact with lipid bilayers and metal cations, thereby altering membrane lipid dynamics and modulating the activity of various membrane-bound proteins (Kagan et al. 2002; Gehman et al. 2008; Bokvist et al. 2004). In this sense, the aggregation state and the structure of the  $\beta$ -peptide in

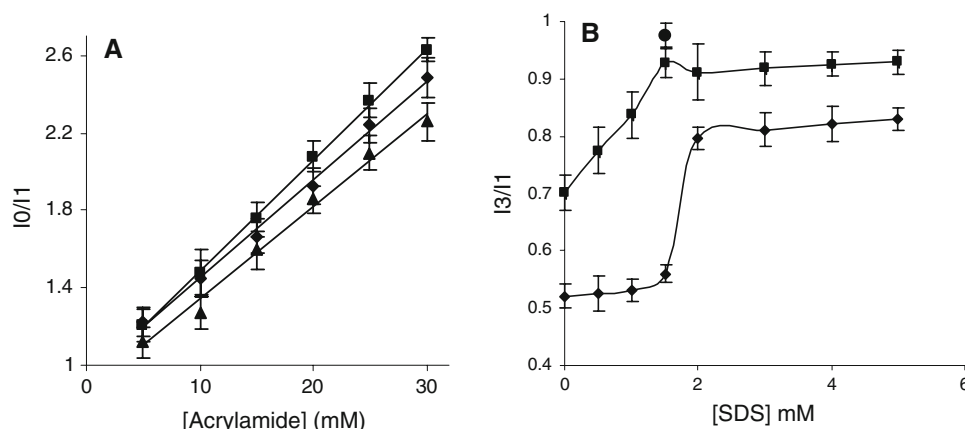


**Fig. 5 a** Solvent accessibility of the single tyrosine residue at position 10 of  $A\beta_{1-42}$  peptide. Emission spectra of  $A\beta_{1-42}$  in PBS were collected at 298 K at a series of quencher concentrations. Samples were excited at 275 nm and emission observed from 290 to 350 nm. Stern–Volmer plots were constructed by plotting the peak intensity in the presence of quencher divided by the peak intensity in the absence of quencher ( $I_0/I$ ) as a function of quencher concentration. Stern–Volmer plot derived from acrylamide quenching of 25  $\mu\text{M}$   $A\beta_{1-42}$  (filled square) and 25  $\mu\text{M}$   $A\beta_{1-42}$  + 1.5 mM SDS (filled circle) following 15 s sonication of the sample (filled triangle). The

continuous lines represent the best fit of the experimental data to the general Stern–Volmer equation. The Stern–Volmer constants ( $K_{SV}$ ) obtained from this analysis are presented in Table 4. **b** effect of SDS on pyrene emission. Emission spectra of  $5 \times 10^{-7}$  M pyrene in the absence (filled diamond) and presence of 25  $\mu\text{M}$   $A\beta_{1-42}$  (<) were recorded at series of SDS concentrations at 298 K. Label (filled circle) represents the peptide in presence of 1.5 mM SDS after sonication. Samples were excited at 335 nm and emission observed from 350 to 500 nm. The  $I_3/I_1$  ratio was extracted from each emission spectrum and plotted against SDS concentration

**Table 4** Acrylamide quenching of the intrinsic tyrosine fluorescence of  $A\beta_{1-42}$

Quencher	Freshly dissolved $A\beta_{1-42}$	$A\beta_{1-42}$ treated with submicellar SDS and sonication	$A\beta_{1-42}$ treated with submicellar SDS and sonication
Acrylamide $K_{SV}$ ( $\text{M}^{-1}$ )	$5.77 \pm 0.2$	$5.11 \pm 0.05$	$4.8 \pm 0.05$

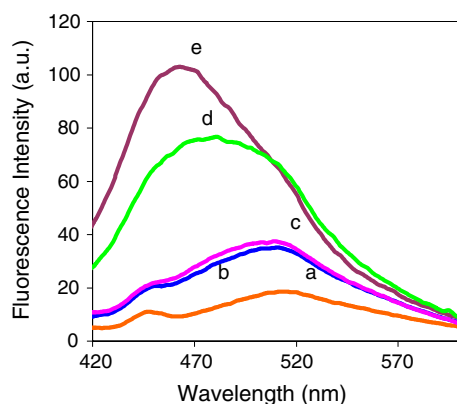


**Fig. 6** Effect of  $A\beta_{1-42}$ /SDS mixtures on ANS fluorescence. Emission spectra were acquired at 298 K. Samples were excited at 375 nm and emission observed from 400 to 600 nm. Data are for  $1 \times 10^{-7}$  M ANS alone (a), and in the presence of 25  $\mu\text{M}$   $A\beta_{1-42}$  (b), 25  $\mu\text{M}$   $A\beta_{1-42}$  previously subjected to sonication, (c) 25  $\mu\text{M}$   $A\beta_{1-42}$  and 1.5 mM SDS (d) and 25  $\mu\text{M}$   $A\beta_{1-42}$  and 1.5 mM SDS previously subjected to sonication (e)

membrane-like environments plays a major role in the development of AD (Arispe et al. 1993).

Various lipid molecules have been reported to induce conformational changes in amyloid-forming proteins, as

well as initiate the formation of oligomeric amyloid precursors (Tew et al. 2008; Morillas et al. 1999; Kakio et al. 2001). Recent advances have shown that  $A\beta_{1-42}$  oligomers play a crucial role in AD progression (Kirkitadze et al. 2002). For instance, cell culture studies demonstrated that secreted amyloid peptides exist in trimeric and tetrameric association states and that these species are present at nanomolar concentrations (Cleary et al. 2005). On association with lipids, these oligomeric peptides developed into spherical, higher order aggregates. Interestingly, it has also been reported that individual phospholipids accelerate  $\beta$ -sheet formation at submicellar concentrations (Danny et al. 2001).

The surfactant molecule SDS has been used to provide some evidence about amyloid and membrane interactions. For example, electron microscopy studies indicate that when treated with 0.5 mM SDS,  $\beta$ 2-microglobulin forms extended fibrils with a helical filamentous morphology (Yamamoto et al. 2004).

We demonstrate here that freshly dissolved  $A\beta_{1-42}$  develops a greater proportion of  $\beta$ -sheet structure upon incubation with submicellar concentrations of SDS. Accordingly, as shown in Figs. 1a, b and 6, it is plausible

that  $A\beta_{1-42}$ , after associating with SDS, develops a partial helical structure whose hydrophobicity induces protein aggregation to reduce the free energy of the system. The evolution of a negative CD peak at 218 nm and IR peaks centred at 1,631 and 1,625  $\text{cm}^{-1}$  support the idea that self-assembled peptides develop more  $\beta$ -sheet structures as a function of submicellar SDS concentration. On the other hand, as shown in Fig. 1a and b, SDS at concentrations higher than the CMC (2.0 mM) causes the  $A\beta_{1-42}$  peptide to form an  $\alpha$ -helix-rich non-amyloidogenic conformer. This is probably due to an increase in SDS micelles. Partial or complete unfolding of the native state is generally believed to be required for amyloid formation (Fandrich et al. 2001). However, recent in vitro studies of  $A\beta$  fibrillogenesis suggest that helix formation precedes the strand formation in protofibrillar assembly. Kirkitadze et al. have observed the formation of oligomeric, helix-containing fibril intermediates in fibrillogenesis of 18 clinically relevant alloforms of  $A\beta$  (Kirkitadze et al. 2001). A similar structural transition from  $\alpha$ -helix to  $\beta$ -sheet was also observed in the non-disease related peptide SCR 3 (18–34) and a 17-residue fragment from human complement receptor CR1 (Clark et al. 1996). Grobner et al. have also seen an increase in  $\alpha$ -helix with  $A\beta(1-40)$  with model membranes (Bokvist et al. 2004).

Recently, it has been shown that sonication of proteins resulted in amorphous aggregates and fibrils with different morphologies. Stathopulos reviewed that sonication of a range of structurally diverse proteins resulted in the formation of aggregates (Stathopulos et al. 2004). This may be due to a sequential process involving the “unzipping” of protective entangled peptide chains, exposure of  $\beta$ -strands, and association of these exposed strands into aggregates. However, sonication of  $A\beta_{1-42}$  peptide in solution in the absence of SDS does not induce any conformational changes as suggested by our CD and ANS results. Presumably sonication increases aggregate–aggregate interactions and forces them into bigger assemblies of 100–200 nm. It should be noted that high hydrophobicity and high  $\beta$ -sheet content are important factors for amyloid like aggregation (Lopez De La Paz et al. 2002). The  $I_3/I_1$  ratio obtained for the peptide–micelle complex (0.93) is greater than that obtained for micelles alone (0.83) indicating that the interior of the peptide–micelle complex is more hydrophobic in nature than that of the SDS micelle. Hence, the interaction between the peptide and the submicellar SDS promotes or stabilizes the formation of secondary structures that lead the folded peptides to self-associate. In the brain, the  $A\beta_{1-42}$  peptide may fold into soluble, monomeric random coil and  $\alpha$ -helical structures, as well as the less soluble, aggregated (oligomeric)  $\beta$ -sheet structure (Choo et al. 1996).

Our observations about the conformational transitions in the  $A\beta_{1-42}$  peptide are summarized in a schematic way in

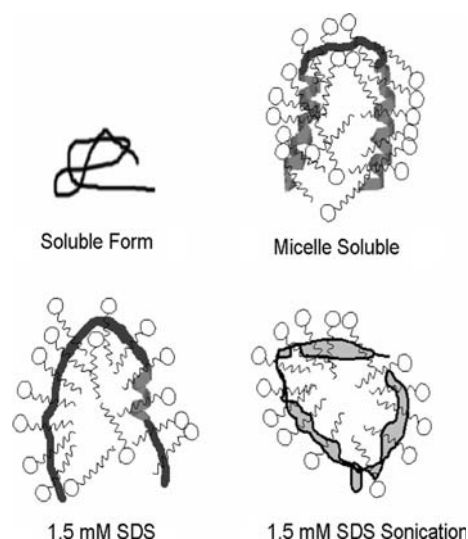


**Fig. 7** Depiction of  $A\beta_{1-42}$  conformation in the presence of submicellar and micellar SDS concentrations

Fig. 7. In the soluble monomeric form, the disordered structure prevails, which on treatment with 1.5 mM SDS adopts an “unzipped” conformation with rudimentary secondary structure. Sonication causes the peptide to rearrange mainly into a  $\beta$ -sheet. Finally, in the presence of SDS micelles, the peptide adopts a predominantly  $\alpha$ -helical structure, as already noted by others in this field (Coles et al. 1998).

## Conclusion

The major finding of this study is that the  $A\beta_{1-42}$  peptide forms small spherical oligomers at submicellar SDS concentrations and that upon sonication, the resulting intermediates act as nuclei to form larger spherical aggregates. The ease at which these large aggregates, composed of numerous loosely packed oligomeric units, form at submicellar SDS concentrations might be due to the relatively low energy requirements needed to reach the partially folded state from the monomeric state. We propose that the formation of a partially folded intermediate and its stability at submicellar SDS concentration are the two major factors involved in the formation of spherical aggregates. At submicellar concentrations, SDS and phospholipids exhibit many similar physicochemical properties (Jao et al. 2004). Considering this, our results contribute to a better understanding of the mechanism underlying the conformational changes induced by membrane lipids in  $A\beta_{1-42}$  peptides and thought to be toxic. This assumes special importance in the light of therapeutic treatments for AD. As Kakio et al. suggested, membrane studies aimed at lowering  $A\beta_{1-42}$  oligomer–lipid interactions will lead to

better therapeutics for the treatment of Alzheimer's disease (Kakio et al. 2001).

**Acknowledgments** We thank Dr. T. Ramasami, Director, CLRI, for his kind support for this work. One of the author, N. Sureshbabu thanks the Council for Scientific and Industrial Research (CSIR) for providing funds in the form of SRF. We also thank Dr. Ganesh, Vanderbilt University, for his help with peptide synthesis.

## References

- Arispe N, Pollard HB, Rojas E (1993) Giant multilevel cation channels formed by Alzheimer disease amyloid beta-protein (A beta P-(1–40)) in bilayer membranes. *Proc Natl Acad Sci USA* 90:10573–10577. doi:10.1073/pnas.90.22.10573
- Bokvist M, Lindstrom F, Watts A, Grobner G (2004) Two types of Alzheimer's beta-amyloid (1–40) peptide membrane interactions: aggregation preventing transmembrane anchoring versus accelerated surface fibril formation. *J Mol Biol* 335:1039–1049. doi:10.1016/j.jmb.2003.11.046
- Booth DR, Sunde M, Bellotti V, Robinson CV, Hutchinson WL, Fraser PE, Hawkins PN, Dobson CM, Radford SE, Blake CC, Pepys MB (1997) Instability, unfolding and aggregation of human lysozyme variants underlying amyloid fibrillogenesis. *Nature* 385:787–793. doi:10.1038/385787a0
- Chaney MO, Webster SD, Kuo YM, Roher AE (1998) Molecular modeling of the Abeta1-42 peptide from Alzheimer's disease. *Protein Eng* 11:761–767. doi:10.1093/protein/11.9.761
- Chen S, Berthelie V, Yang W, Wetzel R (2001) Polyglutamine aggregation behavior in vitro supports a recruitment mechanism of cytotoxicity. *J Mol Biol* 311:173–182. doi:10.1006/jmbi.2001.4850
- Chiti F, Webster P, Taddei N, Clark A, Stefani M, Ramponi G, Dobson CM (1999) Designing conditions for in vitro formation of amyloid protofilaments and fibrils. *Proc Natl Acad Sci USA* 96:3590–3594. doi:10.1073/pnas.96.7.3590
- Choo LPI, Wetzel DL, Halliday W, Jackson M, LeVine SM, Mantsch HH (1996) In situ characterization of  $\beta$ -amyloid in Alzheimer's diseased tissue by synchrotron Fourier transform infrared micro-spectroscopy. *Biophys J* 71:1672–1679
- Clark NS, Dodd I, Mossakowska DE, Smith RA, Gore MG (1996) Folding and conformational studies on SCR1-3 domains of human complement receptor 1. *Protein Eng* 9:877–884. doi:10.1093/protein/9.10.877
- Cleary JP, Walsh DM, Hofmeister JJ, Shankar GM, Kuskowski MA, Selkoe DJ, Ashe KH (2005) Natural oligomers of the amyloid-beta protein specifically disrupt cognitive function. *Nat Neurosci* 8:79–84. doi:10.1038/nn1372
- Coles M, Bicknell W, Watson AA, Fairlie DP, Craik DJ (1998) Solution structure of amyloid beta-peptide (1–40) in a water-micelle environment. Is the membrane-spanning domain where we think it is? *Biochemistry* 37:11064–11077. doi:10.1021/bi972979f
- Crowther DC, Serpell LC, Dafforn TR, Gooptu B, Lomas DA (2003) Nucleation of  $\alpha$  1-antichymotrypsin polymerization. *Biochemistry* 42:2355–2363. doi:10.1021/bi0259305
- Decker H, Ryan M, Jaenicke E, Terwilliger N (2001) SDS-induced phenoloxidase activity of hemocyanins from *Limulus polyphemus*, *Eurypelma californicum*, and *Cancer magister*. *J Biol Chem* 276:17796–17799. doi:10.1074/jbc.M010436200
- Dong A, Prestrelski SJ, Allison SD, Carpenter JFJ (1995) Infrared spectroscopic studies of lyophilization- and temperature-induced protein aggregation. *Pharm Sci* 84:415–424
- Ekiel I, Abrahamson M (1996) Folding-related dimerization of human cystatin C. *J Biol Chem* 271:1314–1321. doi:10.1074/jbc.271.3.1314
- Fandrich M, Fletcher MA, Dobson CM (2001) Amyloid fibrils from muscle myoglobin. *Nature* 410:165–166. doi:10.1038/35065514
- Fezoui Y, Teplow DB (2002) Kinetic studies of amyloid beta-protein fibril assembly. Differential effects of alpha-helix stabilization. *J Biol Chem* 277:36948–36954. doi:10.1074/jbc.M204168200
- Finelli A, Kelkar A, Song HJ, Yang H, Konsolaki M (2004) A model for studying Alzheimer's Abeta42-induced toxicity in *Drosophila melanogaster*. *Mol Cell Neurosci* 26:365–375. doi:10.1016/j.mcn.2004.03.001
- Garavito RM, Ferguson-Miller SJ (2001) Detergents as tools in membrane biochemistry. *J Biol Chem* 276:32403–32406. doi:10.1074/jbc.R100031200
- Gehman JD, O'Brien CC, Shabanpoor F, Wade JD, Separovic F (2008) Metal effects on the membrane interactions of amyloid-beta peptides. *Eur Biophys J* 37:333–344. doi:10.1007/s00249-007-0251-2
- Gong Y, Chang L, Viola KL, Lacor PN, Lambert MP, Finch CE, Krafft GA, Klein WL (2003) Alzheimer's disease-affected brain: presence of oligomeric A $\beta$  ligands (ADDLs) suggests a molecular basis for reversible memory loss. *Proc Natl Acad Sci USA* 18:10417–10422. doi:10.1073/pnas.1834302100
- Guijarro JI, Sunde M, Jones JA, Campbell ID, Dobson CM (1998) Amyloid fibril formation by an SH3 domain. *Proc Natl Acad Sci USA* 95:4224–4228. doi:10.1073/pnas.95.8.4224
- Halverson K, Fraser PE, Kirschner DA Jr, Lansbury PT (1990) Molecular determinants of amyloid deposition in Alzheimer's disease: conformational studies of synthetic beta-protein fragments. *Biochemistry* 29:2639–2644. doi:10.1021/bi00463a003
- Hatters DM, Lawrence LJ, Howlett GJ (2001) Submicellar phospholipid accelerates amyloid formation by apolipoprotein C-II. *FEBS Lett* 494:220–224. doi:10.1016/S0014-5793(01)02355-9
- Jao CC, Der-Sarkissian A, Chen J, Langen R (2004) Structure of membrane-bound -synuclein studied by site-directed spin labeling. *Proc Natl Acad Sci USA* 101:8331–8336. doi:10.1073/pnas.0400553101
- Jen CJ, McIntire LV (1984) Characteristics of shear-induced aggregation in whole blood. *J Lab Clin Med* 103:115–124
- Kagan BL, Hirakura Y, Azimov R, Azimova R, Lin MC (2002) The channel hypothesis of Alzheimer's disease: current status. *Peptides* 23:1311–1315. doi:10.1016/S0196-9781(02)00067-0
- Kakio A, Nishimoto S, Yanagisawa K, Kozutsumi Y, Matsuzaki K (2001) Cholesterol-dependent formation of GM1 ganglioside-bound amyloid  $\beta$ -protein, an endogenous seed for Alzheimer amyloid. *J Biol Chem* 276:24985–24990. doi:10.1074/jbc.M100252200
- Kayed R, Bernhagen J, Greenfield N, Sweimeh K, Brunner H, Voelter W, Kapurniotu AJ (1999) Conformational transitions of islet amyloid polypeptide (IAPP) in amyloid formation in vitro. *Mol Biol* 287:781–796. doi:10.1006/jmbi.1999.2646
- Kelly JW (1998) The alternative conformations of amyloidogenic proteins and their multi-step assembly pathways. *Curr Opin Struct Biol* 8:101–106. doi:10.1016/S0959-440X(98)80016-X
- Kim J, Lee M (2004) Observation of multi-step conformation switching in  $\beta$ -amyloid peptide aggregation by fluorescence resonance energy transfer. *Biochem Biophys Res Commun* 316:393–397
- Kirkitadze MD, Bitan G, Teplow DB (2002) Paradigm shifts in Alzheimer's disease and other neurodegenerative disorders: the emerging role of oligomeric assemblies. *J Neurosci Res* 69:567–577. doi:10.1002/jnr.10328
- Kirkitadze MD, Condron MM, Teplow DB (2001) Identification and characterization of key kinetic intermediates in amyloid beta-protein fibrillogenesis. *J Mol Biol* 312:1103–1119. doi:10.1006/jmbi.2001.4970



- Klein WL (2002) ADDLs & protofibrils—the missing links? *Neurobiol Aging* 23:231–235. doi:[10.1016/S0197-4580\(01\)00312-8](https://doi.org/10.1016/S0197-4580(01)00312-8)
- Lai Z, Colon W, Kelly JW (1996) The acid-mediated denaturation pathway of transthyretin yields a conformational intermediate that can self-assemble into amyloid. *Biochemistry* 35:6470–6482. doi:[10.1021/bi952501g](https://doi.org/10.1021/bi952501g)
- Lambert MP, Stevens G, Sabo S, Barber K, Wang G, Wade W, Krafft G, Snyder S, Holzman TF, Klein WL (1994) Beta/A4-evoked degeneration of differentiated SH-SY5Y human neuroblastoma cells. *J Neurosci Res* 39:377–385. doi:[10.1002/jnr.490390404](https://doi.org/10.1002/jnr.490390404)
- Le Berre F, Chauveteau G, Pefferkorn EJ (1998) Shear induced aggregation/fragmentation of hydrated colloids. *Colloid Interface Sci* 199:13–21. doi:[10.1006/jcis.1997.5308](https://doi.org/10.1006/jcis.1997.5308)
- Lopez De La Paz M, Goldie K, Zurdo J, Lacroix E, Dobson CM, Hoenger H, Serrano L (2002) De novo designed peptide-based amyloid fibrils. *Proc Natl Acad Sci USA* 99:16052–16057. doi:[10.1073/pnas.252340199](https://doi.org/10.1073/pnas.252340199)
- Lougheed WD, Woutfe-Flanagan H, Clement JR, Albisser AM (1980) Insulin aggregation in artificial delivery systems. *Diabetologia* 19:1–9. doi:[10.1007/BF00258302](https://doi.org/10.1007/BF00258302)
- Ma K, Talafous J, Orlando R, Zagorski MG (1997) Trifluoroacetic acid pretreatment reproducibly disaggregates the amyloid  $\beta$ -peptide. *Int J Exp Clin Invest* 4:240–252
- Mark A Thompson, Planaria Software LLC, Seattle, WA <http://www.arguslab.com>
- Matsunaga Y, Ierovnik E, Yamada T, Turk V (2002) Conformational changes preceding amyloid-fibril formation of amyloid-beta and stefin B; parallels in pH dependence. *Curr Med Chem* 9:1717–1724
- Morillas M, Swietnicki W, Gambetti P, Surewicz WKJ (1999) Membrane environment alters the conformational structure of the recombinant human prion protein. *J Biol Chem* 274:36859–36865. doi:[10.1074/jbc.274.52.36859](https://doi.org/10.1074/jbc.274.52.36859)
- Motta A, Andreotti G, Amodeo P, Strazzullo G, Castiglione Morelli MA (1998) Solution structure of human calcitonin in membrane-mimetic environment: the role of the amphipathic helix. *Proteins* 32:314–323. doi:[10.1002/\(SICI\)1097-0134\(19980815\)32:3<314::AID-PROT7>3.0.CO;2-H](https://doi.org/10.1002/(SICI)1097-0134(19980815)32:3<314::AID-PROT7>3.0.CO;2-H)
- Muga A, Arrondo JLR, Bellon T, Sancho J, Bernabeu C (1993) *Arch Biochem Biophys* 300:451–457. doi:[10.1006/abbi.1993.1061](https://doi.org/10.1006/abbi.1993.1061)
- Narayanaswami V, Kim J, McNamee MG (1993) Protein–lipid interactions and *Torpedo californica* nicotinic acetylcholine receptor function. 1. Spatial disposition of cysteine residues in the gamma subunit analyzed by fluorescence-quenching and energy-transfer measurements. *Biochemistry* 32:12413–12419. doi:[10.1021/bi00097a020](https://doi.org/10.1021/bi00097a020)
- Narayanaswami V, Szeto S, Ryan RO (2001) Lipid-association induced N- and C-terminal domain reorganization in human apolipoprotein E3. *J Biol Chem* 276:37853–37860
- O’Nuallain B, Williams AD, Westermark P, Wetzel R (2004) Seeding specificity in amyloid growth induced by heterologous fibrils. *J Biol Chem* 279:17490–17499. doi:[10.1074/jbc.M311300200](https://doi.org/10.1074/jbc.M311300200)
- Pertinhez TA, Bouchard M, Smith RA, Dobson CM, Smith LJ (2002) Stimulation and inhibition of fibril formation by a peptide in the presence of different concentrations of SDS. *FEBS Lett* 529:193–197. doi:[10.1016/S0014-5793\(02\)03333-1](https://doi.org/10.1016/S0014-5793(02)03333-1)
- Prusiner SB (1997) Prion diseases and the BSE crisis. *Science* 278:245–251. doi:[10.1126/science.278.5336.245](https://doi.org/10.1126/science.278.5336.245)
- Ramirez-Alvarado M, Merkel JS, Regan L (2000) A systematic exploration of the influence of the protein stability on amyloid fibril formation in vitro. *Proc Natl Acad Sci USA* 97:8979–8984. doi:[10.1073/pnas.150091797](https://doi.org/10.1073/pnas.150091797)
- Rangachari V, Reed DK, Moore DB, Rosenberry TL (2006) Secondary structure and interfacial aggregation of amyloid- $\beta$ (1–40). *Biochemistry* 45:8639–8648. doi:[10.1021/bi060323t](https://doi.org/10.1021/bi060323t)
- Rangachari V, Moore DB, Reed DK, Sonoda LK, Bridges AW, Conboy E, Hartigan D, Rosenberry TL (2007) Amyloid-beta(1–42) rapidly forms protofibrils and oligomers by distinct pathways in low concentrations of sodium dodecylsulfate. *Biochemistry* 46:12451–12462. doi:[10.1021/bi701213s](https://doi.org/10.1021/bi701213s)
- Rochet JC Jr, Lansbury PT (2000) Amyloid fibrillogenesis: themes and variations. *Curr Opin Struct Biol* 10:60–68. doi:[10.1016/S0959-440X\(99\)00049-4](https://doi.org/10.1016/S0959-440X(99)00049-4)
- Satheeshkumar KS, Jayakumar R (2002) Sonication induced sheet formation at the air–water interface. *Chem Commun (Camb)* 7:2244–2245. doi:[10.1039/b206886a](https://doi.org/10.1039/b206886a)
- Schwyzler R (1986) Molecular mechanism of opioid receptor selection. *Biochemistry* 25:6335–6342. doi:[10.1021/bi00368a075](https://doi.org/10.1021/bi00368a075)
- Selkoe DJ (1996) Amyloid  $\beta$ -protein and the genetics of Alzheimer’s disease. *J Biol Chem* 271:18295–18298
- Shoa H, Jao S, Ma K, Zagorski MG (1999) Solution structure of micelle-bound amyloid  $\beta$ -(1–40) and  $\beta$ -(1–42) peptides of alzheimer’s disease. *J Mol Biol* 285:755–773. doi:[10.1006/jmbi.1998.2348](https://doi.org/10.1006/jmbi.1998.2348)
- Solomon B (2002) Mini Rev. Towards Alzheimer’s disease vaccination. *Med Chem* 2:85–92
- Soto C (2001) Protein misfolding and disease; protein refolding and therapy. *FEBS Lett* 498:204–207. doi:[10.1016/S0014-5793\(01\)02486-3](https://doi.org/10.1016/S0014-5793(01)02486-3)
- Sreerama N, Woody RW (2000) Anal. Estimation of protein secondary structure from circular dichroism spectra: comparison of CONTIN, SELCON, and CDSSTR methods with an expanded reference set. *Biochemistry* 287:252–260
- Stathopoulos PB, Scholz GA, Hwang Y-M, Rumfeldt JAO, Leprock JR, Meiering EM (2004) Sonication of protein causes formation of aggregates that resemble amyloid. *Protein Sci* 13:1–11. doi:[10.1110/ps.03309504](https://doi.org/10.1110/ps.03309504)
- Stryer AL (1978) Fluorescence energy transfer as a spectroscopic ruler. *Rev Biochem* 47:819–846. doi:[10.1146/annurev.bi.47.070178.004131](https://doi.org/10.1146/annurev.bi.47.070178.004131)
- Surewicz WK, Mantsch HH, Chapman D (1993) Determination of protein secondary structure by Fourier transform infrared spectroscopy: a critical assessment. *Biochemistry* 32:389–394. doi:[10.1021/bi00053a001](https://doi.org/10.1021/bi00053a001)
- Terzi E, Holzemann G, Seelig J (1995) Self-association of beta-amyloid peptide (1–40) in solution and binding to lipid membranes. *J Mol Biol* 252:633–642. doi:[10.1006/jmbi.1995.0525](https://doi.org/10.1006/jmbi.1995.0525)
- Tew DJ, Bottomley SP, Smith DP, Cicciotosto GD, Babon J, Hinds MG, Masters CL, Cappai R, Barnham KJ (2008) Stabilization of neurotoxic soluble beta-sheet-rich conformations of the Alzheimer’s disease amyloid-beta peptide. *Biophys J* 94:2752–2766. doi:[10.1529/biophysj.107.119909](https://doi.org/10.1529/biophysj.107.119909)
- Uversky VN, Fink AL (2004) Conformational constraints for amyloid fibrillation: the importance of being unfolded. *Biochim Biophys Acta* 1698:131–153
- Uversky VN, Li J, Fink AL (2001) Evidence for a partially folded intermediate in alpha-synuclein fibril formation. *J Biol Chem* 276:10737–10744. doi:[10.1074/jbc.M010907200](https://doi.org/10.1074/jbc.M010907200)
- Walsh DM, Klyubin I, Fadeeva JV, Rowan MJ, Selkoe DJ (2002) Amyloid-beta oligomers: their production, toxicity and therapeutic inhibition. *Biochem Soc Trans* 30:552–557. doi:[10.1042/BST0300552](https://doi.org/10.1042/BST0300552)
- Waterhous DV Jr, Johnson WC (1994) Importance of environment in determining secondary structure in proteins. *Biochemistry* 33:2121–2128. doi:[10.1021/bi00174a019](https://doi.org/10.1021/bi00174a019)
- Wu P, Li YK, Talalay P, Brand L (1994) Characterization of the three-tyrosine residues of delta 5–3-ketosteroid isomerase by time-resolved fluorescence and circular dichroism. *Biochemistry* 33:7415–7422. doi:[10.1021/bi00189a048](https://doi.org/10.1021/bi00189a048)
- Yamamoto S, Hasegawa K, Yamaguchi I, Tsutsumi S, Kardos J, Goto Y, Gejyo F, Naiki H (2004) Low concentrations of sodium dodecyl sulphate induce the extension of  $\beta$ -microglobulin-related amyloid fibrils at a neutral pH. *Biochemistry* 43:11075–11082. doi:[10.1021/bi049262u](https://doi.org/10.1021/bi049262u)